

RESEARCH

Open Access



# Characterization of phage HZY2308 against *Acinetobacter baumannii* and identification of phage-resistant bacteria

Ruilin Wang<sup>1†</sup>, Xiaojuan You<sup>1†</sup>, Xinwei Liu<sup>1,2</sup>, Bing Fei<sup>1</sup>, Yifan Li<sup>1</sup>, Dan Wang<sup>1</sup>, Rui Zhu<sup>1,2\*</sup> and Yongwei Li<sup>1,2,3,4,5\*</sup>

## Abstract

**Background** *Acinetobacter baumannii* (AB) is a notable cause of hospital-acquired infections, with carbapenem-resistant *Acinetobacter baumannii* (CRAB) classified as a high-priority critical pathogen. Bacteriophage therapy is emerging as a promising alternative to combat drug-resistant bacterial infections. In this study, a lytic phage, HZY2308, was isolated from hospital sewage, and the biological properties, biosafety and anti-biofilm properties of phage HZY2308 were characterized and identified. Moreover, the antibacterial effect of phage HZY2308 in combination with antibiotics was investigated, and the apparent characteristics of phage-resistant strain AB48-R were demonstrated, which provided data support for further studies to elucidate the mechanism of generating phage resistance.

**Methods** Phage HZY2308 was isolated by double agar plate method using clinical strain AB48 as the host bacterium. The morphology of phage HZY2308 was identified by transmission electron microscopy (TEM), and biological characteristics of phage HZY2308 were identified by host range, the efficiency of plating (EOP), sensitivity to temperature, pH, and chloroform, one-step growth curve, the optimal multiplicity of infection (MOI), and detection of endotoxin and cytotoxicity. Besides, the complete genome map of HZY2308 was constructed using CGview, and the phylogenetic tree of HZY2308 was constructed with MEGA. Additionally, the full genomic sequence of phage HZY2308 and the selected phage were compared using Easyfig. Checkerboard test of phage HZY2308 in combination with tigecycline (TGC) was performed to investigate their synergistic effect and bactericidal kinetics. The effect of HZY2308 on biofilm was investigated by semi-quantitative staining of biofilm with crystal violet, determination of bacterial activity in biofilm by 2,3-Bis (2-methoxy-4-nitro-5-sulfophenyl) -2 H-tetrazolium-5-carboxanilide (XTT) assay and observation of biofilm structure by fluorescence microscopy. Finally, Phage-resistant bacteria AB48-R were characterized by colony-forming capacity, morphology, growth curves, adsorption efficiency, and antibiotic susceptibility assays.

<sup>†</sup>Ruilin Wang and Xiaojuan You are co-first authors.

\*Correspondence:

Rui Zhu  
zr4487933891@163.com  
Yongwei Li  
lyw@hactcm.edu.cn

Full list of author information is available at the end of the article



© The Author(s) 2024. **Open Access** This article is licensed under a Creative Commons Attribution-NonCommercial-NoDerivatives 4.0 International License, which permits any non-commercial use, sharing, distribution and reproduction in any medium or format, as long as you give appropriate credit to the original author(s) and the source, provide a link to the Creative Commons licence, and indicate if you modified the licensed material. You do not have permission under this licence to share adapted material derived from this article or parts of it. The images or other third party material in this article are included in the article's Creative Commons licence, unless indicated otherwise in a credit line to the material. If material is not included in the article's Creative Commons licence and your intended use is not permitted by statutory regulation or exceeds the permitted use, you will need to obtain permission directly from the copyright holder. To view a copy of this licence, visit <http://creativecommons.org/licenses/by-nc-nd/4.0/>.

**Results** A lytic phage, HZY2308, was isolated from hospital sewage, which exhibited advantageous traits such as a brief incubation period, large burst size, and robust stability. Safety assessments conducted at both genetic and cellular levels also have yielded positive outcomes. Besides, phage HZY2308 effectively inhibited AB biofilm formation and disrupted established biofilm structures. Furthermore, a synergistic antibacterial effect was noted when phage HZY2308 was combined with tigecycline. Interestingly, the phage-resistant strain, AB48-R was screened through natural selection. Compared to the wild strain AB48, the adsorption efficiency of the phage to AB48-R diminished. However, AB48-R's sensitivity to antibiotics such as cefepime, gentamicin, amikacin, and tobramycin increased, indicating an evolutionary trade-off.

**Conclusions** Phage HZY2308 shows strong antimicrobial potential, especially in combination with tigecycline, and the phage-resistant strain exhibits increased antibiotic sensitivity.

**Keywords** Lytic phage, *Acinetobacter baumannii*, Biofilm, Phage resistance

## Introduction

*Acinetobacter baumannii* (AB) is, a gram-negative, non-fermentative bacterium, recognized as a significant pathogen in hospital-acquired infections. It contributes to a variety of healthcare-associated infections (HAIs) in hospitalized individuals, especially those in intensive care units. These infections include ventilator-associated pneumonia, catheter-associated bloodstream infections, and urinary tract infections [1, 2]. The acquisition and upregulation of drug-resistant genetic elements, such as plasmids, transposons, and integrons, have led to an increased isolation rate of multidrug-resistant AB (MDR-AB) strains. Moreover, the pronounced biofilm formation capacity of AB substantially enhances its resistance to antibiotics [3, 4]. The biofilm formation rate of AB has been reported to range from 80 to 91%, which is significantly higher than that of other species (5–24%) [5].

Carbapenems are currently utilized as  $\beta$ -lactam antibiotics with broad-spectrum antibacterial activity and are considered the last line of defense in treating MDR bacterial infections [6]. In 2024, the World Health Organization (WHO) designated Carbapenem-resistant AB (CRAB) as the highest priority pathogen urgently requiring novel antibiotics [7]. According to data from the China Antimicrobial Surveillance Network (CHINET), in 2023, the resistance rates of clinical AB strains to imipenem and meropenem were 73.4% and 73.7%, respectively. The mortality rate among patients with CRAB-related infections, including bloodstream infections and hospital-acquired pneumonia, exceeded 60%, underscoring the urgent need for innovative anti-infection strategies to replace traditional antibiotics [8].

Phages are a class of viruses that specifically infect and lyse bacteria, with 20–40% of bacterial lysis attributed to phages. Historically, phages played a role in treating bacterial infections before being superseded by antibiotic therapy. Given the escalating global challenge of bacterial resistance, phage therapy has attracted renewed attention [9, 10]. Phages are categorized into lytic and lysogenic types based on their ability to lyse host bacteria [11].

Lytic phages infect bacteria through processes including adsorption, penetration, biosynthesis, maturation, and release of phage particles [12]. Receptor-binding proteins (RBPs) at the distal end of the phage tail bind specifically to receptor proteins on the bacterial surface, determining the phage's host range [13]. After invading a host cell, temperate phages can integrate nucleic acids into the host's chromosomes. As the host cell replicates synchronously, it does not cause the lysis of the host cell. Meanwhile, it often carries and expresses genes that influence bacterial physiology, pathogenicity, metabolism, and sensitivity to other phages [14, 15]. Typically, only lytic phages are employed in phage therapy, a rapidly advancing field. Compared to antibiotics, phage therapy offers advantages such as high specificity, efficiency, robust self-replication, and ease of genetic manipulation [16, 17].

Narrow host range and phage resistance are the main obstacles limiting the application of single phage therapy. Phage resistance can occur at every stage of a phage life cycle, and the mechanisms are complex and diverse [18, 19], including modification or loss of the phage receptor [20].

In this study, the clinical isolate AB48 served as the host bacteria for isolating lytic phage HZY2308 from hospital sewage. The phage demonstrated a broad host range, high lysing activity, safety, and excellent anti-biofilm activity. Furthermore, the combination of phage and tigecycline (TGC) exhibited a synergistic antibacterial effect. We also isolated the phage-resistant strain AB48-R and characterized its morphology, adsorption efficiency, and antibiotic sensitivity, providing data support for the potential application of phage HZY2308 as a novel antimicrobial agent.

## Materials and methods

### Bacterial strain

All clinical AB strains, including AB48 (GeneBank accession number: CP155446) were isolated and identified by the Clinical Laboratory of Henan Provincial Hospital of Traditional Chinese Medicine (TCM) and stored in 30%

(V/V) glycerol at  $-80^{\circ}\text{C}$ . After performing a three-section streak on the blood plate, the strains were cultured in a  $37^{\circ}\text{C}$ , 5%  $\text{CO}_2$  incubator for 24 h for resuscitation. A single colony was inoculated into Luria-Bertani (LB) liquid medium and shaken at  $37^{\circ}\text{C}$ , 160 rpm, until the culture reached the logarithmic phase with Optical Density (OD) 600 around 0.6–1.0.

### Isolation and purification of phage HZY2308

Phage isolation, purification, and characterization were performed with modifications to the method [21]. The untreated hospital sewage was collected and left for 2 h at  $4^{\circ}\text{C}$ , centrifuged at 8000 rpm for 10 min, and the supernatant was filtered through a  $0.22\ \mu\text{m}$  filter (Millipore, United States). The supernatant was mixed with a volume  $2\times$ LB broth medium, and 100  $\mu\text{L}$  of host bacterium AB48 (OD<sub>600</sub>=0.5) was added. The mixture was cultured with shaking ( $37^{\circ}\text{C}$ , 200 rpm) and centrifuged (5000 rpm, 10 min) after clarification. The supernatant was filtered by a  $0.22\ \mu\text{m}$  filter to obtain a phage stock solution. The phage HZY2308 (GeneBank accession number: OR730450) was purified using a double-layer agar plate method (1.5% agar at the bottom and 1.0% agar at the top) until plaques of uniform size and morphology were obtained.

### Morphological observation of phage HZY2308

The agar-containing phage was soaked in PBS buffer at  $4^{\circ}\text{C}$  for 4 h, then centrifuged and filtered to obtain sterile supernatant. The phage was centrifuged in a 30 kD ultrafiltration tube (Millipore, United States) ( $4^{\circ}\text{C}$ ,  $3000\times g$ , 20 min). The phage was fixed on 200-mesh carbon-coated copper grids and stained with 2% (W/V) phosphotungstic acid (PTA). The phage was observed using Hitachi HT7800 TEM.

### The optimal multiplicity of infection (MOI) of phage HZY2308

Phage HZY2308 and AB48 were mixed at different MOI values (10, 1, 0.1, 0.01, 0.001) and cultured in shaking ( $37^{\circ}\text{C}$ , 180 rpm) for 4 h. The mixture was centrifuged (5000 rpm, 10 min) and then filtered to remove bacteria. The double agar plate method was used to determine phage titer, and the MOI with the highest titer was the optimal MOI of phage HZY2308. The experiment was repeated three times.

### One-step growth curve of phage HZY2308

According to the method of Fei et al. [22], phage HZY2308 was mixed with AB48 at MOI=0.01, incubated at  $37^{\circ}\text{C}$  for 15 min and then centrifuged ( $4^{\circ}\text{C}$ ,  $10000\times g$ , 5 min). The precipitate was re-suspended with LB liquid medium and cultured ( $37^{\circ}\text{C}$ , 160 rpm) for 100 min. The

phage titer was measured by double agar plate method every 10 min. The experiment was repeated three times.

### Determination of temperature, pH and chloroform sensitivity of phage HZY2308

500  $\mu\text{L}$  of phage HZY2308 ( $\sim 10^{10}$  PFU/mL) was incubated at various temperatures (4, 25, 37, 50, 60, 70,  $80^{\circ}\text{C}$ ) for 1 h. Phage HZY2308 ( $\sim 10^{10}$  PFU/mL) was mixed with SM buffers of different pH values (3, 5, 7, 9, 10, 11, and 13) at a ratio of 1:10 (v/v) and incubated at  $37^{\circ}\text{C}$  for 1 h. Phage HZY2308 was also mixed with chloroform solution at a ratio of 1:10 (v/v) and incubated at  $37^{\circ}\text{C}$  for 1 h. The phage titer was determined using the double-layer agar plate method. The experiment was repeated three times.

### Determination of phage host range

The host range of phage was determined by the spot test assays. The bacterial suspension was adjusted to OD<sub>600</sub> of 0.5 and spread on LB solid agar plates. Subsequently, 10  $\mu\text{L}$  of phage HZY2308 ( $\sim 10^{10}$  PFU/mL) was dropped to the plates, which were then incubated at  $37^{\circ}\text{C}$  overnight. “++” indicated that clear phage plaques were formed. “+” indicated that phage plaques were formed but were faint. “-” indicated that no phage plaques were formed. The experiment was repeated three times.

### Determination of phage HZY2308 efficiency of plating (EOP)

The infectivity of phage HZY2308 was evaluated by determining its efficiency of plating (EOP) based on spotting assay results within its host range. Phage stock solutions were prepared at four concentrations ( $10^7$ ,  $10^8$ ,  $10^9$ , and  $10^{10}$  PFU/mL) with three replicates per concentration. The double-layer agar plate method was used to measure phage-induced lysis of target bacteria, and the number of plaque-forming units (PFUs) was calculated.  $\text{EOP} = (\text{average PFU on target bacteria} / \text{average PFU on host bacteria}) \pm$  the standard deviation for the three measurements [23]. EOP values of 0.5 or higher were classified as “high production”, meaning target bacteria produced at least 50% of the PFUs compared to host bacteria. The EOP between 0.1 and 0.5 was considered “medium production”. The EOP between 0.001 and 0.1 was considered “low production”, while the EOP of less than 0.001 was categorized as inefficient [24]. The experiment was repeated three times.

### Detection of endotoxin in phage HZY2308

The endotoxin content of the phage solution was determined using the procedures outlined in the endotoxin ELISA kit (Shanghai YuanYe Bio-Technology Co., Ltd., China). Using the software Origin, a linear regression curve was constructed with the standard concentration

on the horizontal axis and the OD450 values on the vertical axis. From this curve, the endotoxin content of phage HZY2308 was calculated. The experiment was repeated three times.

#### Detection of cytotoxicity in phage HZY2308

THP-1, a cell line derived from human acute monocytic leukemia, was used to assess the cytotoxicity of the phage HZY2308. THP-1 cells were seeded into a 96-well plate at a density of  $4 \times 10^4$  cells per well, with the addition of Phorbol 12-myristate 13-acetate (PMA, Beijing Solarbio Science & Technology Co., Ltd., China) to a final concentration of 200 ng/mL. The cells were cultured overnight at 37 °C with 5% CO<sub>2</sub> to induce differentiation into macrophages. Phage HZY2308 was diluted in a ten-fold gradient using Roswell Park Memorial Institute 1640 (RPMI-1640) supplemented with 10% fetal bovine serum (FBS), ranging from  $10^8$  to  $10^{14}$  PFU/mL, and subsequently added to the cells. The cells were incubated at 37 °C and 5% CO<sub>2</sub> for 24, 48, and 72 h. Following two washes with sterile PBS, each well received 90 µL of PBS and 10 µL of Cell Counting Kit-8 (CCK-8, Beyotime Biotechnology Co., Ltd., China) solution and was incubated for an additional 4 h before the OD450 nm was measured. The experiment was repeated three times.

#### Phage genome extraction

Phage DNA was extracted using the Viral Gene Extraction Kit (Takara Biomedical Technology Co., Ltd., China). A total of 200 µL of Buffer VGB, 20 µL of Proteinase K, and 1.0 µL of Carrier RNA were added to 200 µL of phage stock solution ( $\geq 10^8$  PFU/mL). The mixture was incubated in a 56 °C water bath for 10 min, followed by the addition of 200 µL of anhydrous ethanol and thorough mixing by pipetting. The solution was then transferred to a Spin Column placed on a Collection Tube and centrifuged at 12,000 rpm for 2 min. The filtrate was discarded. Next, 500 µL of Buffer RWA was added to the Spin Column, followed by centrifugation at 12,000 rpm for 1 min, and the filtrate was discarded. Then, 700 µL of Buffer RWB was added, and the Spin Column was centrifuged again at 12,000 rpm for 1 min, with the filtrate discarded. This step was repeated once, followed by centrifugation at 12,000 rpm for 2 min, and discarding the filtrate afterward. The Spin Column was transferred to a new 1.5 mL RNase-free collection tube. To elute the DNA, 30~50 µL of RNase-free ddH<sub>2</sub>O was added to the center of the Spin Column membrane. After allowing it to stand at room temperature for 5 min, the column was centrifuged at 12,000 rpm for 2 min to collect the DNA.

#### Genome sequencing and annotation of phage HZY2308

The phage DNA was sequenced using the Illumina HiSeq 2500 sequencer, resulting in the acquisition of

the complete genome sequence. This DNA sequence was uploaded to the National Center for Biotechnology Information (NCBI) for a Basic Local Alignment Search Tool (BLASTn; <https://blast.ncbi.nlm.nih.gov/Blast.cgi>) analysis, and the result was compared with other phages in the GenBank database to identify similar phages. The tRNA genes encoded by the phage were searched using tRNAscan-SE (<http://lowelab.ucsc.edu/tRNAscan-SE/>). Gene annotation for the phage-encoded genes was performed using the Rapid Annotations using Subsystems Technology (RAST, <https://rast.nmpdr.org/>). The predicted amino acid sequences of these genes were analyzed for function using NCBI's protein BLAST (BLASTp). Virulence factors and antibiotic resistance were predicted using the Virulence Factor Database (VFDB; <http://www.mgc.ac.cn/VFs/>) and the Antibiotic Resistance Genes Database (ARDB; <https://card.mcmaster.ca/>). The complete genomic map of the phage was illustrated using CGview (<https://proksee.ca/>).

#### Affinity analysis of phage HZY2308

Phylogenetic analysis was conducted based on the highly conserved sequences of the terminal enzyme large subunits from various phages. The amino acid sequence encoded by the large subunit of the terminal enzyme of phage HZY2308 was entered into NCBI's BLASTp. Ten sequences with significant homology were selected. These sequences were then used to build a phylogenetic tree using the ClustalW tool within MEGA11.0 software. Additionally, the full genomic sequences of phage HZY2308 and the selected phage were compared using Easyfig.

#### Checkerboard test of phage HZY2308 in combination with tigecycline

Due to the ongoing evolutionary arms race between bacteria and phages, therapies using a single phage type often led to the emergence of phage-resistant strains. In this investigation, phage HZY2308 was combined with TGC (Beijing Solarbio Science & Technology Co., Ltd., China) to evaluate its bacterial inhibition efficacy. A modified checkerboard test was used to determine a combination of phage HZY2308 and TGC [25, 26]. In the horizontal rows of a 96-well plate, 50 µL of TGC at concentrations of 2, 1, 0.5, 0.25, 0.125, 0.0625, 0.03125, and 0.015625 µg/mL were added. Vertically, 50 µL aliquots containing phage HZY2308 at multiplicity of infections (MOIs) of 100, 10, 1, 0.1 and 0.01 were added. Each well was then supplemented with 100 µL of AB48 bacteria diluted to  $1 \times 10^6$  CFU/mL for the experimental group. The bacterial control group received 100 µL of AB culture and 100 µL of LB broth, while the blank control group was supplemented with 200 µL of LB broth. After 24 h incubation at 37 °C, 20 µL of bladed azure solution

was added. The fractional inhibitory concentration (FIC) was calculated as follows: FIC of drug A ( $FIC_A$ ) = MIC of drug A in combination / MIC of drug A alone. Synergistic effects were indicated by an FIC index less than 0.5; additive effects were denoted by an FIC index of 0.5 to 1; indifferent effects were characterized by an FIC index greater than 1 and less than 2; and antagonistic effects were reflected by an FIC index of 2 or higher. The experiment was repeated three times.

#### Antibacterial activity of phage HZY2308 and TGC

The bactericidal kinetics of phage HZY2308 in combination with TGC were assessed using 96-well plates. The experimental design included several groups: a bacterial control group, a phage-only group (MOI=0.01), TGC-only groups at concentrations of 1/2 MIC and 1/32 MIC, and combination groups of phage HZY2308 (MOI=0.01) with TGC (1/2 MIC and 1/32 MIC). The bacterial strain AB48 was adjusted to a concentration of  $1 \times 10^6$  CFU/mL. For each well, 100  $\mu$ L of this bacterial suspension was added, followed by the addition of 100  $\mu$ L of phage and/or TGC, both diluted in LB broth, according to the specified group. The contents were gently mixed and the plate was incubated at 37 °C. The optical density at 600 nm (OD600) was measured hourly over a 24 h period to monitor bacterial growth inhibition. The bactericidal curves were plotted with time on the horizontal axis and OD600 values on the vertical axis to illustrate the dynamics of bacterial inhibition. The experiment was repeated three times.

#### The measurement of biofilm amount by Crystal violet assay.

The assay was performed according to the literature method with minor modifications [27]. To observe the effect of phage HZY2308 on AB48 biofilm formation, 100  $\mu$ L of AB48 ( $\sim 10^6$  CFU/mL) and 100  $\mu$ L of phage HZY2308 at a multiplicity of infection (MOI) of 0.01 were added to a 96-well plate and incubated at 37 °C for 24, 48, and 72 h, respectively. Additionally, 100  $\mu$ L of AB48 was inoculated into the wells and incubated at 37 °C for 24, 48, and 72 h to form biofilms. Subsequently, phage HZY2308 was added at an MOI of 0.01 and incubated for an additional 24 h to investigate its effect on disrupting mature biofilms. After the designated incubation periods, the wells were washed with PBS to remove planktonic bacteria. The biofilms were fixed with methanol for 30 min and then stained with 0.1% crystal violet solution (Shanghai Biotech Biological Co., Ltd., China) for 20 min. The excess stain was washed away with PBS, and 250  $\mu$ L of 33% glacial acetic acid was added to each well to dissolve the crystal violet. The absorbance was measured at 595 nm. The experiment was repeated three times.

#### The measurement of bactericidal activity in biofilms by XTT assay

The assay method referred to a previous study with partial modification [22], after the designated incubation period, the wells were washed with PBS to remove planktonic bacteria. Subsequently, 200  $\mu$ L of LB medium and 20  $\mu$ L of XTT working solution (Shanghai YuanYe Bio-Technology Co., Ltd., China) were added to each well. The plates were incubated in the dark at 37 °C for 3 h. The absorbance was then measured at 490 nm. The inhibition rate of the phage on bacteria within the biofilm was calculated using the following formula:

$$\left[ 1 - \frac{A(\text{Experimental group}) - A(\text{Blank control group})}{A(\text{Control group}) - A(\text{Blank control group})} \right] \times 100\%.$$

The experiment was repeated three times.

#### The observation of biofilm structures using fluorescence microscopy

Referring to the above method for determining the formation and destruction of AB48 biofilm by phage HZY2308 using 96-well plates, phage HZY2308 and AB48 were added to a 12-well plate at an MOI of 0.01, and glass slides (25 mm  $\times$  25 mm) were placed in the wells. The plate was incubated at 37 °C for 24, 48, and 72 h. The slides were then removed, and planktonic bacteria were washed off with PBS. The biofilms were fixed with 4% formaldehyde (Shanghai YuanYe Bio-Technology Co., Ltd., China) for 15 min, rinsed with PBS, and air-dried. Subsequently, the biofilms were stained with 0.02% acridine orange solution in the dark at room temperature for 15 min. The slides were washed with PBS to remove unbound dye, air-dried, and observed under a fluorescence microscopy to examine the biofilm structure. The experiment was repeated three times.

#### Screening of phage-resistant bacteria

After culturing AB48 with phage HZY2308 at an MOI of 0.01 in LB medium for 24 h, the culture was streaked onto blood agar plates using an inoculating loop, then isolated several single colonies and performed three successive rounds of purification. The bacterial strains were identified using a bacterial identification mass spectrometer. Plaque assays and spot tests were conducted to determine if the bacteria have developed resistance to the phage. Gram staining was performed on both AB48 and phage-resistant bacteria, followed by observation of their bacterial morphology under an oil immersion microscopy.

#### Determination of growth curve

AB48 and phage-resistant bacteria in the logarithmic growth phase were diluted to  $1.0 \times 10^6$  CFU/mL. 100  $\mu$ L of the bacterial suspension and 100  $\mu$ L of LB medium

were added to each well of a 96-well plate and incubated statically at 37 °C. OD600 was measured every hour for 24 h. A bactericidal curve was plotted with time on the x-axis and OD600 values on the y-axis. The experiment was repeated three times.

#### Determination of adsorption efficiency

AB48 and the phage-resistant bacteria were each mixed with phage HZY2308 at MOI of 0.01 and incubated at 37 °C for 15 min. The mixture was then centrifuged at 8000 rpm for 10 min at 4 °C. The supernatant was filtered through a 0.22 µm filter, and the phage titer in the supernatant was determined using the double-layer agar plate method. The adsorption efficiency was calculated using the following formula: Adsorption efficiency = [(initial phage titer - phage titer in the supernatant) / initial phage titer] × 100%. The experiment was repeated three times.

#### Antibiotic sensitivity test

The VITEK-2 Compact automatic microbiological analyzer Antimicrobial Susceptibility Testing-Gram-Negative (AST-GN) card (BioMérieux, France) was used for routine antimicrobial susceptibility testing. Susceptibility results were interpreted following the Clinical and Laboratory Standards Institute (CLSI) guidelines.

#### Statistical analysis

GraphPad Prism 8.0 was used for statistical analysis of the results. Multiple groups were analysed using one-way analysis of variance or two-way analysis of variance. Significance was indicated by \* $P < 0.05$ , \*\* $P < 0.01$ , \*\*\* $P < 0.001$ , and \*\*\*\* $P < 0.0001$ .

## Results

#### Isolation and morphology of phage HZY2308

A phage was isolated from hospital sewage using AB48 as the host bacterium. After three rounds of purification, the phage formed transparent, clear, and uniform plaques with a diameter of approximately 2.0 mm on a double agar plate. These were accompanied by a diffuse halo with a diameter of about 6.0 mm (Fig. 1A). TEM revealed that the phage head had a polygonal structure with a diameter of approximately 70 nm, and it possessed a tail of approximately 110 nm in length. The tail was encased in a semi-retractable sheath with a diameter of about 20 nm and a baseplate with a diameter of approximately 60 nm (Fig. 1B). The phage was named HZY2308 (GeneBank accession number: OR730450) and classified within the *Caudovirales*.

#### Biological characterization and biosafety analysis of phage HZY2308

The stability of phages under different conditions of temperature and pH must be evaluated to ensure their efficacy in clinical applications. Phage HZY2308 exhibited peak activity within the temperature range of 4 to 50 °C. There was no statistically significant difference in phage titer within this range. However, the titer decreased sharply at 60 °C and the phage completely lost activity at 80 °C (Fig. 2A). Phage HZY2308 demonstrated optimal biological activity when the pH was between 5.0 and 9.0. However, the phage titer declined rapidly at pH levels  $\geq 11.0$  or  $\leq 3.0$  (Fig. 2B). Moreover, chloroform treatment did not affect the titer of phage HZY2308, suggesting the absence or minimal presence of lipid constituents in the phage capsids (Fig. 2F). The variation in phage titer across different MOIs was assessed using the

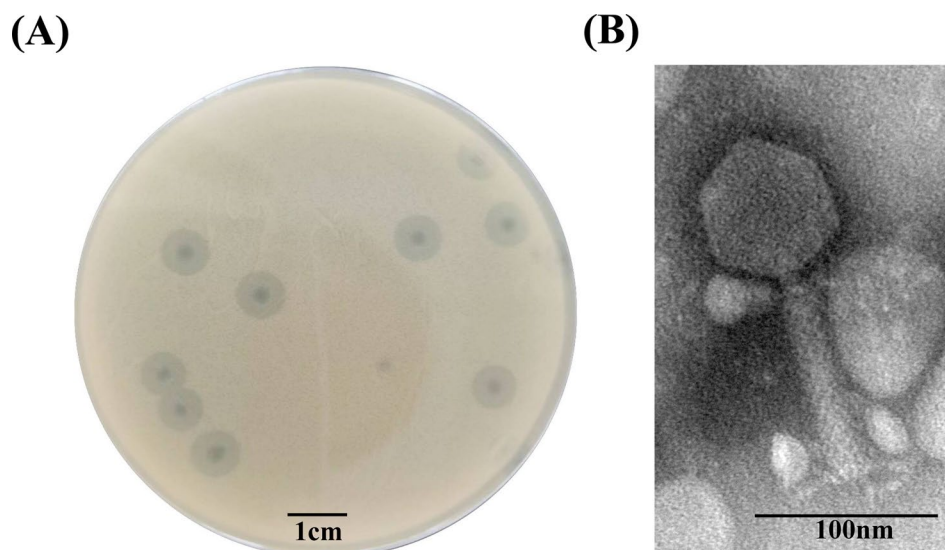


**Fig. 1** Morphology of phage HZY2308. (A) Phage spot morphology of phage HZY2308. (B) Electron microscopy morphology of phage HZY2308.

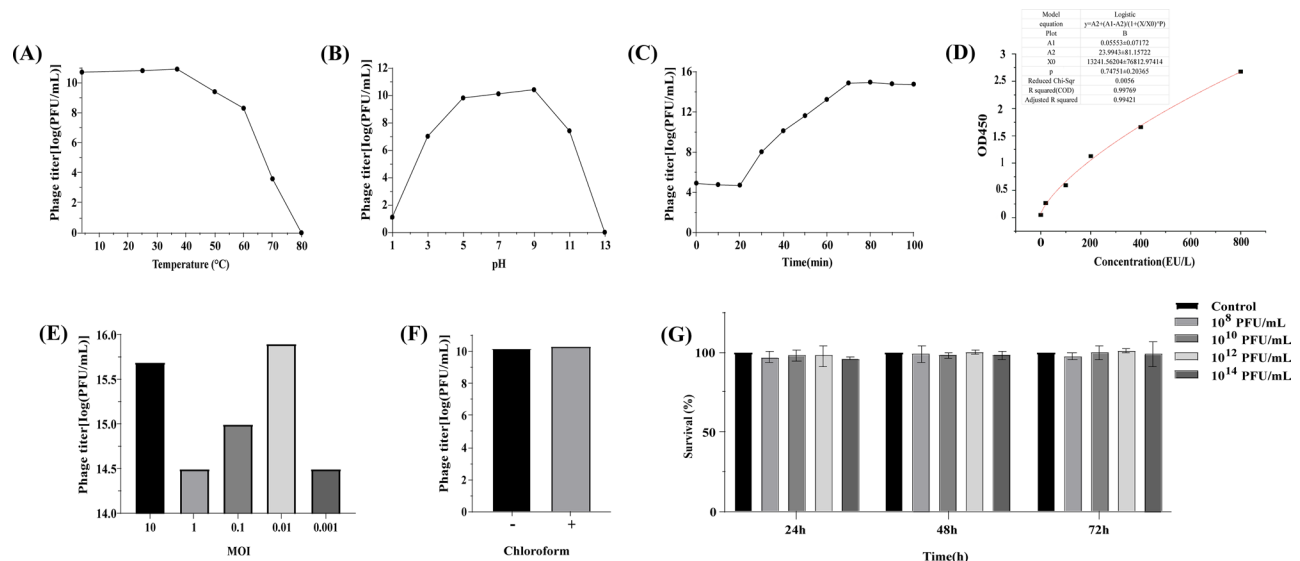


**Fig. 2** Biological characterization and biosafety analysis of phage HZY2308. **(A)** Determination of temperature stability of phage HZY2308. **(B)** Determination of pH stability of phage HZY2308. **(C)** One-step growth curve of phage HZY2308. **(D)** Detection of endotoxin in phage HZY2308. **(E)** The optimal multiplicity of infection (MOI) of phage HZY2308. **(F)** Determination of chloroform sensitivity of phage HZY2308. **(G)** Detection of cytotoxicity in phage HZY2308. Data were expressed as mean  $\pm$  SD ( $n=3$ ).

double-layer agar plate method. Results indicated that at an MOI of 0.01, phage HZY2308 reached a titer of  $8.2 \times 10^{15}$  PFU/mL, which was identified as the optimal MOI (Fig. 2E). The one-step growth curve demonstrated that phage HZY2308 had a latent period of approximately 20 min and a burst size of about  $4 \times 10^6$  PFU per infected cell. The multiplication period plateaued at 70 min, highlighting the rapid lysis capability of phage HZY2308 (Fig. 2C). A drop test was conducted to determine the host range of phage HZY2308 against 43 AB strains (including 33 CRAB strains, Table 1). This test revealed that HZY2308 lysed 39.53% (17/43) of the strains and 42.42% (14/33) of CRAB strains, the EOP demonstrated a productive infection rate of 76.47% (13/17) for phage HZY2308, with a high production rate of 35.29% (6/17) (Table 1). These findings highlighted the potential of phage HZY2308 as a candidate antibacterial agent for CRAB infections.

The endotoxin level in the phage solution was quantified via ELISA, revealing an average endotoxin content of 49.80 EU/ $10^7$  PFU, significantly below the quality control threshold of 250 EU/ $10^7$  PFU (Fig. 2D). The safety of phage HZY2308 on mammalian cell of THP-1 was assessed using the CCK-8 assay. The result revealed no cytotoxic effects after 24, 48, and 72 h of co-culture with THP-1 cells at varying phage titers (Fig. 2G), thus confirming the cellular safety of phage HZY2308 (See Table 2).

### Genome analysis of phage HZY2308

The sequencing and analysis of the complete genome of phage HZY2308 revealed a circular double-stranded

DNA molecule with a length of 45,720 base pairs and a GC content of 37.9%. Comparative genomic analysis via BLASTn with *Acinetobacter* phage NJ02 (GenBank: OR126895.1) indicated that phage HZY2308 shared a 99.13% sequence identity at 86% coverage. The RAST toolkit predicted eighty-eight open reading frames (ORFs) in the genome of HZY2308, with twelve located on the sense strand and seventy-six on the anti-sense strand. These ORFs encoded for various proteins, including fifteen associated with phage structure (e.g., head proteins ORF5 and ORF71; capsid proteins ORF80, ORF81, and ORF82; baseplate proteins ORF58 ORF59, ORF61, and ORF62; tail proteins ORF55, ORF56, ORF67, and ORF69; and other structural proteins ORF63 and ORF78), three linked to phage packaging (terminases ORF7 and ORF8, and portal protein ORF6), five involved in host lysis (superinfection immunity protein ORF28, endolysin ORF52, holin ORF54, and lysozymes ORF65 and ORF66), seven related to DNA replication, repair, and metabolism (including DNA-binding helix-turn-helix structural domain protein ORF15, DNA endonucleases ORF20, ORF40, and ORF47, replicative DNA helicase ORF33, DNA replication protein ORF34, and DNA recombination repair protein ORF46), four associated with phage transcription and translation (anti-repressor protein ORF36, transcriptional regulators ORF42 and ORF72, and RNA polymerase ORF74), two additional proteins (nucleotide triphosphate hydrolyase ORF50 and a DUF2612 domain-containing protein ORF57) (See Table 2), and fifty-two proteins of unknown function. Neither the ARDB nor the VFDB databases predicted the presence of antibiotic-resistance genes or

**Table 1** Cleavage spectrum and the EOP of phage HZY2308

Bacterial strain	Origin	Phage(cleavage ability)	EOP
AB7	Sputum	-	
AB8	Alveolar lavage fluid	-	
AB19	Alveolar lavage fluid	-	
AB20	Sputum	++	0.0088±0.0011
AB35	Sputum	-	
AB39	Sputum	-	
AB45	Sputum	+	1.5378±0.0997
AB50	Alveolar lavage fluid	+	0.1474±0.0253
AB53	Sputum	-	
AB55	Sputum	-	
CRAB1	Sputum	-	
CRAB2	Sputum	+	<0.001
CRAB3	Alveolar lavage fluid	++	<0.001
CRAB5	Pus secretion	-	
CRAB6	Throat swab	-	
CRAB9	Blood	-	
CRAB11	Alveolar lavage fluid	++	0.0842±0.0427
CRAB13	Sputum	-	
CRAB14	Alveolar lavage fluid	+	0.1832±0.0487
CRAB18	Sputum	-	
CRAB21	Sputum	-	
CRAB26	Alveolar lavage fluid	-	
CRAB27	Sputum	+	<0.001
CRAB29	Blood	-	
CRAB30	Sputum	++	1.5445±0.2997
CRAB33	Sputum	+	<0.001
CRAB34	Alveolar lavage fluid	-	
CRAB36	Sputum	-	
CRAB37	Sputum	++	0.0950±0.0344
CRAB38	Sputum	-	
CRAB40	Blood	-	
CRAB41	Sputum	++	0.0011±0.0002
CRAB42	Sputum	++	0.0077±0.0020
CRAB43	Alveolar lavage fluid	+	0.0104±0.0019
CRAB44	Alveolar lavage fluid	-	
CRAB46	Alveolar lavage fluid	-	
CRAB47	Sputum	++	1.8539±0.5452
CRAB49	Alveolar lavage fluid	-	
CRAB51	Sputum	++	1.0323±0.7946
CRAB52	Alveolar lavage fluid	++	1.4935±0.4941
CRAB57	Blood	-	
CRAB63	Sputum	-	
CRAB64	Sputum	-	

Note: “++” indicated that clear phage plaques were formed; “+” indicated that phage plaques were formed but were faint; and “-” indicated that no phage plaques were formed. EOP values of 0.5 or higher were classified as “high production”, meaning target bacteria produced at least 50% of the PFUs compared to host bacteria; The EOP between 0.1 and 0.5 was considered “medium production”; The EOP between 0.001 and 0.1 was considered “Low production”; while the EOP of less than 0.001 was categorized as inefficient.

virulence factors within the genome of HZY2308. All analyses and predictions were visualized using Proksee software (Fig. 3A).

The highly conserved phage terminase large subunit was selected from HZY2308 to construct a phylogenetic tree (Fig. 3B). Phylogenetic analysis indicated that phage HZY2308 was closely related to phages WCHABP12 and Abp9, suggesting that these phages may belong to the same genus. A homology analysis of the complete genomes of phages HZJ2308, WCHABP12, and Abp9 performed by Easyfig revealed the homology among all three phages (Fig. 3C).

#### Anti-biofilm effects of the phage HZY2308

Previous studies have established a strong correlation between the development of drug resistance and biofilm formation in AB [28–30]. In this study, we evaluated the anti-biofilm efficacy of phage HZY2308 against AB48 by quantifying the total biofilm mass, enumerating viable bacteria within the biofilm, and examining biofilm architecture. Compared to the bacterial control group, treatment with phage HZY2308 significantly reduced the total biofilm mass of AB48 after 24, 48, and 72 h ( $P<0.05$ ) (Fig. 4A). Correspondingly, the enumeration revealed a substantial decrease in the number of viable bacteria, with inhibition rates at 24, 48, and 72 h of 84.91%, 74.25%, and 73.20%, respectively ( $P<0.05$ ) (Fig. 4B). Fluorescence microscopy showed that the biofilm structure in the control group was dense and three-dimensional, whereas the biofilm treated with phage HZY2308 appeared more fragmented, displaying a network-like or scattered distribution with fewer bacteria clustering together (Fig. 4C).

Following phage treatment, mature biofilms exhibited significant structural damage ( $P<0.05$ ), as evidenced by the compromised integrity of the biofilm structure (Fig. 4D). The inhibition rates of bacteria within the biofilms at 24, 48, and 72 h were 89.53%, 82.55%, and 61.45%, respectively ( $P<0.05$ ) (Fig. 4E). Additionally, the biofilm structure transitioned to a looser, more dispersed network arrangement, indicating that phage HZY2308 was effective in eradicating mature biofilms (Fig. 4F).

#### Synergistic antibacterial effect of phage HZY2308 combined with TGC

The sensitivity of AB48 to TGC was determined by measuring the minimum inhibitory concentration (MIC) using the broth microdilution method, which was established at 0.5 µg/mL for TGC. However, when combined with phage HZY2308, the MIC was notably decreased, suggesting that the phage-drug combination enhanced bacterial inhibition (Fig. 4G). The synergy between phage HZY2308 and TGC was quantified using the fractional inhibitory concentration (FIC) index, with calculated values at or below 0.5, indicating a synergistic

**Table 2** Phage HZY2308 annotated with functional proteins (GeneBank accession number: OR730450)

No.	Strand	Start position	Stop position	Nucleotide length	Amino-acid size	Predicted function	Similar species	Identified
ORF5	-	1592	2362	771	256	Head morphogenesis	Acinetobacter phage LZ35	99.61%
ORF6	-	2365	3795	1431	476	Portal protein	Acinetobacter phage WCHABP12	100.00%
ORF7	-	3798	5099	1302	433	Terminase large subunit	Acinetobacter phage WCHABP13	100.00%
ORF8	-	5080	5511	432	143	Terminase small subunit	Acinetobacter phage AP22	98.60%
ORF15	-	6944	7144	201	66	Helix-turn-helix domain-containing protein	Escherichia coli	100.00%
ORF20	-	8287	8649	363	120	RusA family crossover junction endodexyribonuclease	Acinetobacter phage WCHABP12	100.00%
ORF28	-	11,677	11,889	213	70	Superinfection immunity protein	Acinetobacter phage WCHABP12	100.00%
ORF33	-	12,871	14,172	1302	433	Replicative DNA helicase	Acinetobacter phage Abp9	99.77%
ORF34	-	14,172	14,927	756	251	DNA replication protein	Acinetobacter phage Brutus	90.04%
ORF36	-	15,149	15,862	714	237	Anti-repressor Ant	Acinetobacter phage WCHABP12	100.00%
ORF40	+	17,064	17,651	588	195	HNH endonuclease	Acinetobacter phage LZ35	100.00%
ORF42	+	17,998	18,810	813	270	Putative transcriptional regulator	Acinetobacter phage LZ35	100.00%
ORF46	+	19,738	20,637	900	299	Recombinase RecT	Escherichia coli	100.00%
ORF47	+	20,634	21,389	756	251	Exonuclease	Acinetobacter phage vB_AbaM_AB3P2	99.20%
ORF50	+	21,843	22,376	534	177	Putative nucleoside triphosphate pyrophosphohydrolase	Acinetobacter phage vB_AbM_WUUPSU	61.38%
ORF52	-	22,692	23,300	609	202	Endolysin	Acinetobacter phage WCHABP12	100.00%
ORF54	-	23,546	23,866	321	106	Holin	Acinetobacter phage Cato	98.11%
ORF55	-	23,942	26,140	2199	732	Tail fiber protein	Acinetobacter phage WCHABP12	99.86%
ORF56	-	26,154	26,999	846	281	Tail fiber protein	Acinetobacter phage vB_AbaM-IME-AB2	95.73%
ORF57	-	26,992	27,618	627	208	DUF2612 domain-containing protein	Escherichia coli	97.12%
ORF58	-	27,618	28,802	1185	394	Baseplate J/gp47 family protein	Acinetobacter phage LZ35	99.75%
ORF59	-	28,799	29,152	354	117	Baseplate wedge subunit	Acinetobacter phage AP22	98.29%
ORF61	-	29,298	29,942	645	214	Baseplate assembly protein	Acinetobacter phage WCHABP1	96.73%
ORF62	-	29,923	30,813	891	296	Baseplate hub	Acinetobacter phage LZ35	100.00%
ORF63	-	30,923	31,198	276	296	Virion structural protein	Acinetobacter phage LZ35	100.00%
ORF65	-	31,820	33,868	2049	682	Putative tail-fiber/lysozyme protein	Acinetobacter phage Ab31	84.53%
ORF66	-	33,871	34,083	213	70	Putative tail-fiber/lysozyme protein	Acinetobacter phage YMC-13-01-C62	90.00%
ORF67	-	34,113	34,538	426	141	Tail assembly chaperone protein	Acinetobacter phage Scipio	99.29%
ORF69	-	35,046	36,509	1464	487	Tail sheath	Acinetobacter phage WCHABP1	98.56%
ORF71	-	36,990	37,553	564	187	Head protein	Acinetobacter phage WCHABP1	100.00%
ORF72	-	37,528	38,199	672	223	Transcriptional regulator	Acinetobacter phage WCHABP1	100.00%
ORF74	-	38,489	38,926	438	145	Putative RNA polymerase	Acinetobacter phage BUCT629	97.93%
ORF78	-	40,050	40,502	453	150	Virion structural protein	Acinetobacter phage LZ35	100.00%
ORF80	-	40,934	41,926	993	330	Major capsid protein	Acinetobacter phage Scipio	99.70%
ORF81	-	41,937	42,431	495	164	Capsid stabilizing protein	Acinetobacter phage Scipio	100.00%
ORF82	-	42,431	43,789	1359	452	Prohead core protein protease	Acinetobacter phage Scipio	100%

effect. Subsequently, phage HZY2308 was administered with TGC at concentrations of 1/2 MIC and 1/32 MIC for a 24 h dynamic inhibition study. This analysis demonstrated that the combination produced a greater inhibitory effect than TGC alone. Initially, the phage-only treatment mirrored the efficacy of the combination therapy up to 13 h, post 13 h, however, its effectiveness decreased (Fig. 4H). This decline suggested the onset

of phage resistance, highlighting that the combination therapy could extend the period before resistance development.

#### Screening and characterization of phage-resistant bacterial strains

Phage HZY2308 was co-cultured with the host bacterium AB48 (MOI=0.01) for 24 h, a phage-resistant strain,

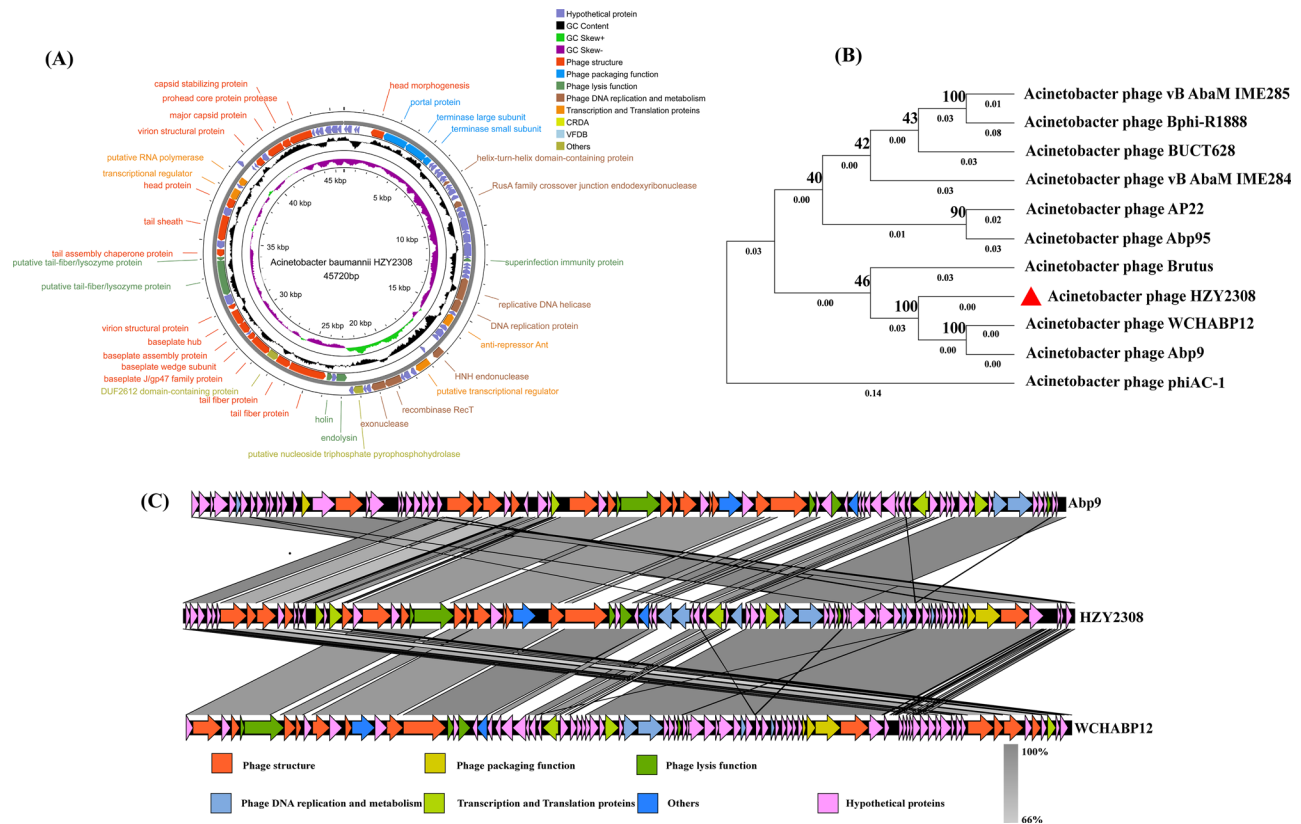


**Fig. 3** Genome analysis of phage HZY2308. **(A)** CGview mapping of phage HZY2308 genome. **(B)** Phylogenetic tree of phage HZY2308 terminase large subunit. The phylogenetic tree was drawn using MEGA (version 11.0.11) using the neighbor-joining (N-J) method with a Bootstrap value of 1000. **(C)** Homology analysis of phage Bbp9, HZY2308, and WCHABP12. Shades of color in the middle-shaded areas represented the degree of homology, and arrow colors represented different functions

AB48-R was isolated, following inoculation on a blood agar plate and three successive passages. Plaque assays confirmed that AB48-R was not lysed by phage HZY2308 after subculturing (Fig. 5A). The colonies of AB48 and AB48-R on the blood agar plate were consistent in size, color, and luster, appearing as white, round formations with well-defined edges. Gram staining revealed the bacteria as eosin colored, predominantly bulbous, and either scattered or paired (Fig. 5B). The growth dynamics of AB48 and AB48-R were assessed by measuring OD600nm values, with results indicating no statistically significant differences in growth rates between the two strains at any time point (Fig. 5C). The initial step in phage infection, adsorption to the bacterial surface, was examined. This study measured the adsorption efficiency of phage HZY2308 to AB48 and AB48-R. The adsorption efficiency for AB48 was 54%, but it decreased to 25% for AB48-R (Fig. 5D). We hypothesized that the resistance of AB48-R to phage HZY2308 might be due to the loss or mutation of the adsorption receptor on the bacterial surface.

The antibiotic susceptibility profiles of AB48 and AB48-R, determined by the Vitek 2 Compact system,

were presented in Table 3. AB48 was sensitive to TGC, colistin, and trimethoprim/sulfamethoxazole, and resistant to other antibiotics. In contrast, AB48-R showed altered susceptibility, shifting from resistant to sensitive for amikacin and tobramycin, and from resistant to intermediate for cefepime and gentamicin. Additionally, the MIC values for imipenem and ciprofloxacin were determined for both strains. The MIC for imipenem was 1 mg/mL for AB48, but decreased to 0.25 mg/mL for AB48-R. Conversely, the MIC for ciprofloxacin was 0.25 mg/mL for AB48, but increased to over 1 mg/mL for AB48-R (Fig. 5E).

## Discussion

Multidrug resistance is one of the prominent features of AB infection [31]. According to the U.S. Centers for Disease Control and Prevention, the incidence of multidrug resistance of AB is 4 times that of other gram-negative bacteria such as *Klebsiella pneumoniae* and *Pseudomonas aeruginosa* [32]. The drug resistance of AB has been associated with increased mortality rates and poses challenges for effective treatment in clinical infections [33], highlighting the pressing need for the development of

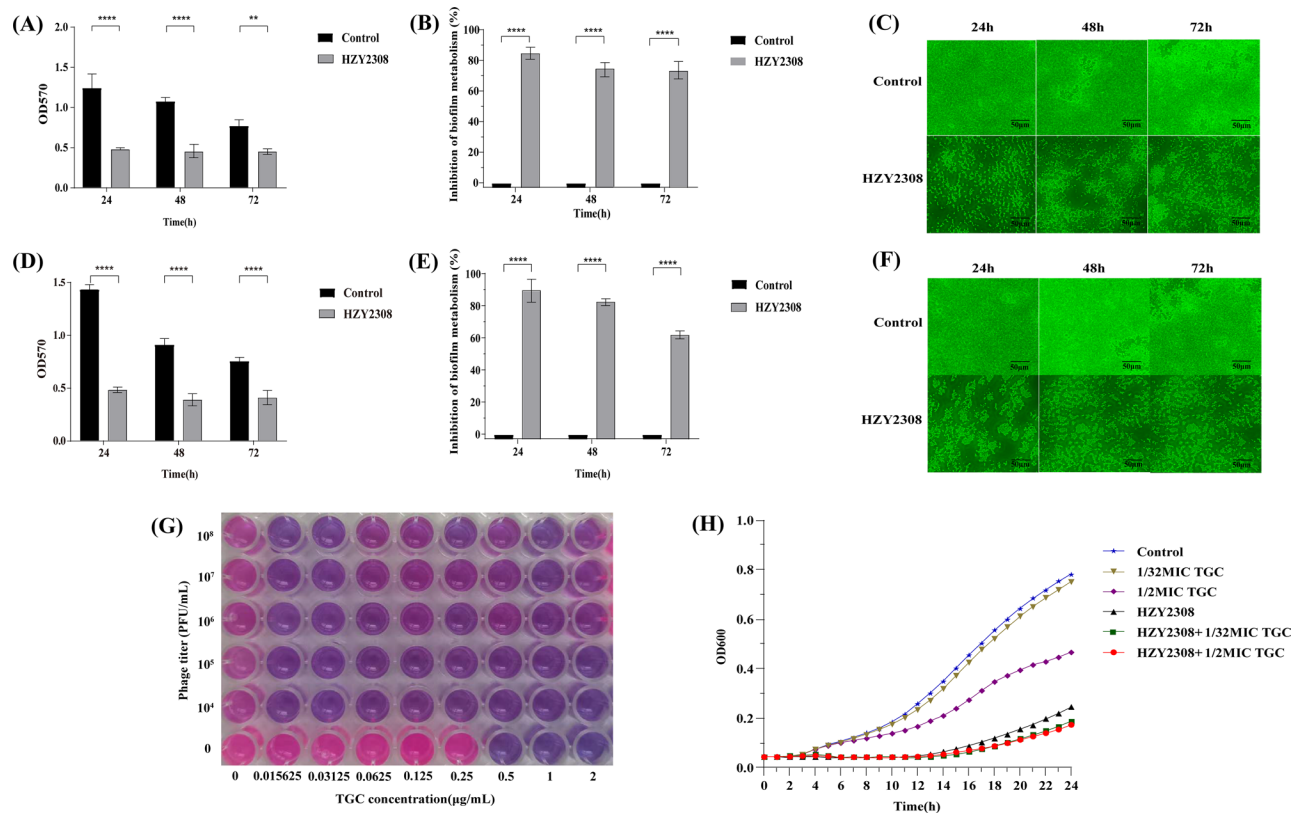


**Fig. 4** Inhibition and disruption of biofilm formation by phage HZY2308 and antimicrobial effect in combination with tigecycline. Inhibition of biofilm formation by phage HZY2308: **(A)** Crystal violet staining to semi-quantify the amount of biofilm at different time points. **(B)** Bacterial activity in biofilm at different time points by XTT reduction method. **(C)** Biofilm structure at different time points under fluorescence microscope; Biofilm disruption by phage HZY2308: **(D)** Crystal violet staining to semi-quantify the amount of biofilm at different time points. **(E)** Bacterial activity in biofilm at different time points by XTT reduction method. **(F)** Biofilm structure at different time points under a fluorescence microscope. **(G)** Checkerboard analysis of phage HZY2308 in combination with tigecycline. **(H)** Inhibition curves of HZY2308, TGC, and HZY2308 + TGC acting on AB48. Data are expressed as mean  $\pm$  SD ( $n=3$ ). (\*\*\*\* indicated  $P < 0.01$ , \*\*\*\*\* indicated  $P < 0.0001$ )

novel antibacterial agents targeting this pathogen. Due to the high host specificity and good biosafety, lytic phage has become a natural antibiotic substitute, attracting people's attention in the treatment of severe bacterial infections [10]. In 2017, the U.S. Food and Drug Administration (FDA) approved the first phage therapy study for treating patients with AB infections [34]. Subsequently, Wu et al. [35] successfully treated four patients with secondary AB infection in the intensive care unit by administering phage cocktails ( $\phi$ Ab121 and  $\phi$ Ab124). Rao et al. [36] adopted phage AbW4878 $\phi$ 1 with broad-spectrum antibiotics, significantly improving clinical symptoms in patients with ventilator-associated pneumonia caused by MDR-AB after 21 days of treatment via nebulization and intravenous injection. Nir-Paz et al. [37] used phage  $\phi$ AbKT21phi3 (for extensively drug-resistance AB, XDR-AB),  $\phi$ KpKT21phi1 (for MDR *Klebsiella pneumoniae*), meropenem, and colistin in combination for the treatment of patients with trauma-associated bacterial infections of the left tibia after observing their antimicrobial effects in vitro, and satisfactory results were obtained.

The narrow host range is one of the obstacles of phage therapy [38]. In this study, we isolated a broad host range phage HZY2308, with a retractable tail. The lysis rate of phage HZY2308 to AB isolates was 39.53% (17/43), with a notably higher rate observed for CRAB strains at 42.42% (14/33), and the EOP demonstrated a high and medium production rate of 47.06% (8/17) for phage HZY2308. Compared with other AB phages [39, 40], this phage had a shorter incubation period, larger burst size, and higher adsorption rate, suggesting that HZY2308 is a promising candidate for the treatment of CRAB infection. Our results showed that phage HZY2308 was stable under different pH and temperature conditions, did not show any cytotoxic effect on THP-1, and its endotoxin content was much lower than the FDA's recommended dose of endotoxin in an intravenous solution [41]. In addition, no antibiotic resistance genes, virulence factor genes, and lysogenicity genes were found to be carried in the genome of phage HZY2308, which proved the safety of phage HZY2308 application at the genetic level.

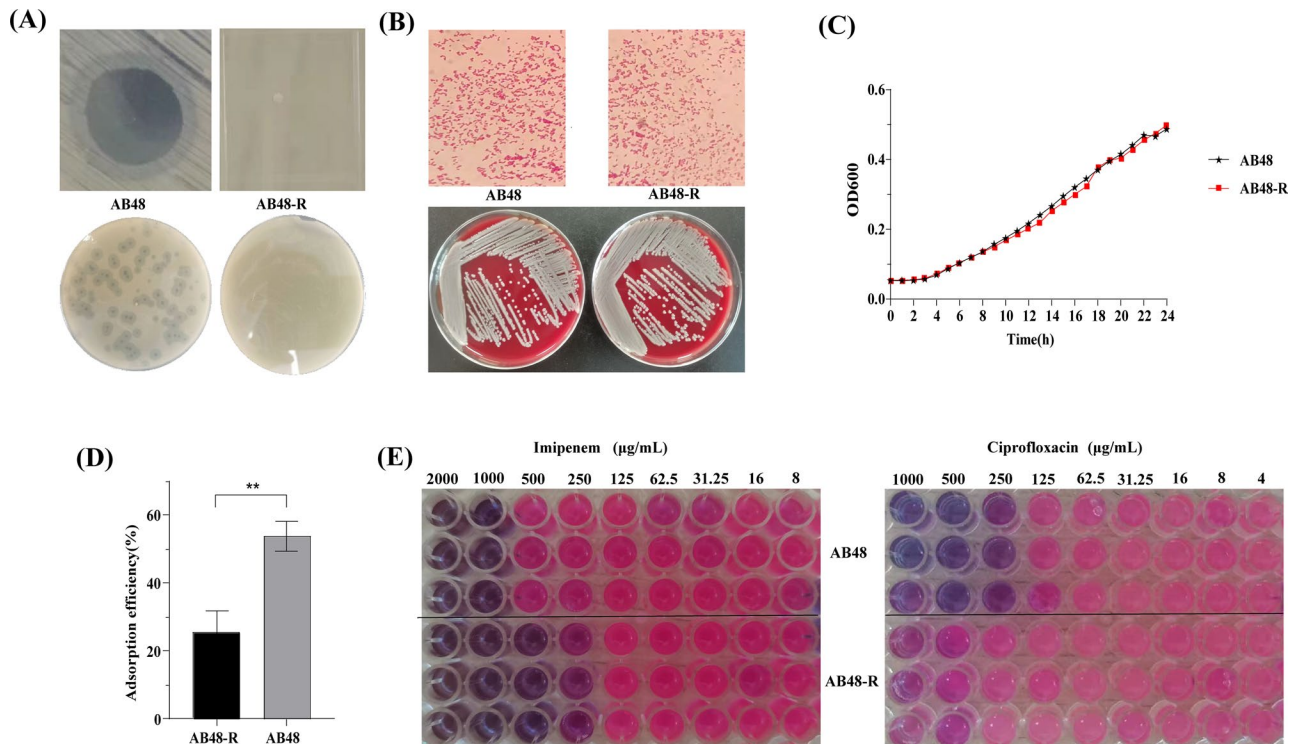


**Fig. 5** Identification of phage HZY2308 resistant strains. **(A)** Empty spot test (upper picture) and spot test (bottom picture) of AB48 vs. AB48-R. **(B)** Comparison of colony and bacterial morphology of AB48 vs. AB48-R. **(C)** The growth curves of AB48 vs. AB48-R. **(D)** The adsorption efficiencies of AB48 vs. AB48-R. **(E)** The antibiotic sensitivity of AB48 vs. AB48-R (\*\*\*) indicated  $P < 0.01$

**Table 3** Comparison of antibiotic susceptibility between AB48 and AB48-R

Antibiotics	AB48		AB48-R	
	MIC	S/I/R	MIC	S/I/R
Piperacillin	≥ 128	R	≥ 128	R
Ampicillin/sulbactam	≥ 32	R	≥ 32	R
Ticacillin/covelaricaci	≥ 128	R	≥ 128	R
Piperacillin/Tazobacta	≥ 128	R	≥ 128	R
Ceftazidime	≥ 64	R	≥ 64	R
Cefoperazone/Sulbactam	≥ 64	R	≥ 64	R
Cefepime	≥ 32	R	16	I
Ceftriaxone	≥ 64	R	≥ 64	R
Imipenem	≥ 16	R	≥ 16	R
Meropenem	≥ 16	R	≥ 16	R
Gentamicin	≥ 16	R	8	I
Amikacin	≥ 64	R	≤ 16	S
Tobramycin	≥ 16	R	≤ 1	S
Ciprofloxacin	≥ 4	R	≥ 4	R
Levofloxacin	≥ 8	R	≥ 8	R
Doxycycline	≥ 16	R	≥ 16	R
Tigacycline	2	S	2	S
Colistin	≤ 0.5	S	2	S
Trimethoprim/sulfamisoazole	≤ 20	S	≤ 20	S

Note: S: Sensitivity; I: Intermediary; R: Resistance

The mechanisms of drug resistance in AB are complex, with biofilm formation being a significant contributor [42]. A biofilm is a highly structured aggregate of micro-colonies formed by bacteria on both living and non-living surfaces to adapt to their environment. It is composed of macromolecular substances such as exopolysaccharides (EPS), extracellular proteins, and extracellular DNA produced by bacteria [43]. AB exhibits a strong ability to form biofilms [4, 44]. Phages, as viruses that specifically lyse bacteria, have increasingly been shown to be a novel and effective strategy for biofilm control [45, 46]. Jiang et al. [47] found that phage vB\_AbaM-SHI alone could effectively inhibit the biofilm formation of AB. In this study, phage HZY2308 not only significantly inhibited the formation of AB48 biofilms but also disrupted the mature biofilm structure, achieving a lysis rate of over 60% for bacteria within the biofilm ( $P < 0.05$ ). This indicated that phage HZY2308 might be a promising antibacterial agent for controlling AB biofilm infections.

Phages can penetrate the extracellular matrix of bacterial biofilms and destroy them by encoding and secreting endolysins, holins, and virion-associated peptidoglycan hydrolases (VAPGHs) [48–50]. Endolysins are cell wall peptidoglycan hydrolases encoded by phages, utilized by most dsDNA phages to degrade the cell wall peptidoglycan layer and release progeny phages [27]. The endolysin Abtn-4, encoded by AB phage D2, has been shown

to reduce biofilm formation [51]. Phage endolysins LysAm24, LysAp22, LysECD7, and LysSi3 have demonstrated efficacy against biofilms with high matrix content (*Klebsiella pneumoniae*), low matrix content (AB), and dual-species biofilms, resulting in at least a twofold reduction in biofilm mass [52]. Holin is a small molecule transmembrane hydrophobic protein that is crucial for endolysins to enter the periplasm [53]. It was found that compared to phage PEF771, phage holin pEF191 exhibited a superior effect in eliminating biofilms [54]. The genes ORF52, encoding endolysin, and ORF54, encoding perforin, were identified in the genome of phage HZY2308. These genes might contribute to the high bactericidal activity of phage HZY2308, including against biofilms, but further confirmations are required.

Given the increasing antibiotic resistance and the limitations of using phages alone, the combination of phages and antibiotics can enhance the burst size of phages, inhibit the development of phage-resistant strains, and reduce antibiotic resistance. Colistin, polymyxins, and TGC are the last-resort treatments for CRAB infections. However, conventional doses of TGC cannot achieve the blood concentrations necessary to treat bloodstream infections, and higher doses are associated with hepatorenal toxicity and the development of drug resistance [55, 56]. In recent years, there have been reports of clinical failures and the emergence of drug resistance during treatment with polymyxins (B and E) [57]. The combinations of the phage KARL-1 with meropenem and colistin, respectively, have significant antibacterial effects on MDR-AB isolates [58]. A patient with hospital-acquired pneumonia caused by CRAB was treated with a combination of an individualized phage preparation, TGC, and polymyxin E. After 16 days of continuous aerosolized treatment, pathogen clearance and significant improvement in lung function were observed [59]. In this study, phage HZY2308 also exhibited excellent antimicrobial effects when combined with TGC, with fractional inhibitory concentration (FIC) values equal to or less than 0.5, suggesting a synergistic bactericidal effect between phage HZY2308 and TGC.

A major obstacle to phage therapy is that single phage therapy can easily lead to the development of phage resistance, thereby diminishing its therapeutic efficacy [60]. In this study, the adsorption efficiency of the phage to the phage-resistant strain AB48-R was significantly reduced compared to AB48 (Fig. 5D). Adsorption is the initial stage of phage infection. Phages recognize the host surface receptor via receptor-binding proteins (RBPs), which are typically located at the end of the phage tail fiber [61]. Inhibition of phage adsorption through deletion or structural alteration of phage receptors is the initial step in bacterial defense against phage infection [62]. The capsule is the most common receptor for phage adsorption

of AB [63, 64]. Gordillo Altamirano F et al. [65] found that after incubation with phages  $\Phi$ FG02 and  $\Phi$ CO01, *A. baumannii* strains AB900 and A9844 exhibited single nucleotide deletions at the K site (capsule biosynthesis locus) [66], resulting in the generation of phage resistant mutants lacking capsule. Wang et al. [67] demonstrated through adsorption tests that the capsule was the primary receptor for Phab24, while the outer membrane served as a secondary receptor. Additionally, they found that Phab24-resistant strains regained their sensitivity to colistin. AB48-R exhibited a shift in susceptibility from resistant (R) to sensitive (S) to amikacin and tobramycin, and from resistant (R) to intermediate (I) to cefepime and gentamicin. Under phage selection pressure, a strong trade-off exists between phage resistance and antibiotic sensitivity. Specifically, when bacteria alter one trait to improve fitness, they often exhibit decreased fitness in another trait [68]. Phages can utilize the outer membrane protein OprM of the MexAB and MexXY efflux pump systems as a receptor-binding site. *Pseudomonas aeruginosa*, in turn, alters the structure of its efflux pump protein to prevent phage adsorption, resulting in increased sensitivity to several antibiotics [69]. The mechanism underlying the change in antibiotic sensitivity of AB48-R has not been determined and requires further investigation. In conclusion, the evolutionary trade-off between the development of phage-resistant bacteria and antibiotic resistance may be an effective target for controlling antibiotic-resistant bacterial infections.

## Conclusion

In this study, we isolated a broad-host-range phage, HZY2308, which efficiently lysed CRAB strains. Phage HZY2308 demonstrated significant anti-biofilm activity, and the combination with antibiotics enhanced the antibacterial effect, indicating its potential as an antibacterial agent to control AB infections.

## Author contributions

R.W: Investigation, Methodology, Software, Data curation, Writing – original draft, Writing – review & editing; X.Y: Methodology, Writing – original draft, Writing – review & editing; X.L: Writing – review & editing. B. F: Methodology; Y.L: Investigation, Writing – review & editing; D. W: Methodology, Writing – review & editing; R.Z: Writing – review & editing, Supervision, Funding acquisition; W.L: Writing – review & editing, Supervision, Funding acquisition.

## Funding

The work was supported by the Henan Provincial Science and Technology Research Project (No. 232102310153 and 242102310148), the Key Scientific Research project of Henan Higher Education Institutions (No.24A310007), the Natural Science Foundation of Henan Province (No.242300420437), Henan University of Chinese Medicine 2023 annual postgraduate research and innovation ability improvement plan project (2023KYCX050), and Wu Jieping Medical Foundation (320.6750.2024-03-27).

## Data availability

No datasets were generated or analysed during the current study.

## Declarations

### Ethical approval

Not applicable.

### Competing interests

The authors declare no competing interests.

### Author details

<sup>1</sup>The Second Clinical Medical College of Henan University of Chinese Medicine, Zhengzhou 450002, China

<sup>2</sup>The Second Affiliated Hospital of Henan University of Chinese Medicine, Henan Province Hospital of Traditional Chinese Medicine, Zhengzhou 450002, China

<sup>3</sup>The Key Laboratory of Pathogenic Microbes & Antimicrobial Resistance Surveillance of Zhengzhou, Zhengzhou 450002, China

<sup>4</sup>Henan Engineering Research Center for Identification of Pathogenic Microbes, Zhengzhou 450002, China

<sup>5</sup>Henan Provincial Key Laboratory of Antibiotics-Resistant Bacterial Infection Prevention & Therapy with Traditional Chinese Medicine, Zhengzhou 450002, China

Received: 22 June 2024 / Accepted: 25 October 2024

Published online: 07 November 2024

## References

- Jiang Y, Ding Y, Wei Y, Jian C, Liu J, Zeng Z. Carbapenem-resistant *Acinetobacter baumannii*: a challenge in the intensive care unit. *Front Microbiol.* 2022;13:1045206.
- Mardiana M, Teh S-H, Lin L-C, Lin N-T. Isolation and characterization of a Novel Siphoviridae phage, vB\_AbaS\_TCUP2199, infecting Multidrug-Resistant *Acinetobacter baumannii*. *Viruses.* 2022;14:1240.
- Wang L, Chen Q-W, Qin Y-C, Yi X-L, Zeng H. Analysis of carbapenem-resistant *Acinetobacter baumannii* carbapenemase gene distribution and biofilm formation. *Int J Mol Epidemiol Genet.* 2024;15:1–11.
- Bagińska N, Grygiel I, Orwat F, Harhala MA, Jędrusiak A, Gebarowska E, et al. Stability study in selected conditions and biofilm-reducing activity of phages active against drug-resistant *Acinetobacter baumannii*. *Sci Rep.* 2024;14:4285.
- Sung JY. Molecular characterization and Antimicrobial susceptibility of Biofilm-forming *Acinetobacter baumannii* Clinical isolates from Daejeon, Korea. *Korean J Clin Lab Sci.* 2018;50:100–9.
- El-Gamal MI, Brahim I, Hisham N, Aladdin R, Mohammed H, Bahaeldin A. Recent updates of carbapenem antibiotics. *Eur J Med Chem.* 2017;131:185–95.
- Aggarwal R, Mahajan P, Pandiya S, Bajaj A, Verma SK, Yadav P et al. Antibiotic resistance: a global crisis, problems and solutions. *Crit Rev Microbiol.* 2024;50:1–26.
- Tb DW, Ra N. B, P P, B L, B S. Clinical and pathophysiological overview of *Acinetobacter* infections: a century of challenges. *Clin Microbiol Rev* [Internet]. 2017 [cited 2024 Apr 18];30. <https://pubmed.ncbi.nlm.nih.gov/27974412/>
- Jault P, Leclerc T, Jennes S, Pirnay JP, Que Y-A, Resch G, et al. Efficacy and tolerability of a cocktail of bacteriophages to treat burn wounds infected by *Pseudomonas aeruginosa* (PhagoBurn): a randomised, controlled, double-blind phase 1/2 trial. *Lancet Infect Dis.* 2019;19:35–45.
- Uytendroek S, Chen B, Onsea J, Ruythooren F, Debaveye Y, Devolder D, et al. Safety and efficacy of phage therapy in difficult-to-treat infections: a systematic review. *Lancet Infect Dis.* 2022;22:e208–20.
- Kasman LM, Porter LD. Bacteriophages. *StatPearls* [Internet]. Treasure Island (FL): StatPearls Publishing; 2024 [cited 2024 Apr 17]. <http://www.ncbi.nlm.nih.gov/books/NBK493185/>
- Suttle CA. Marine viruses—major players in the global ecosystem. *Nat Rev Microbiol.* 2007;5:801–12.
- King AMQ, Adams MJ, Carstens EB, Lefkowitz EJ, editors. Order - Caudovirales. *Virus taxonomy* [Internet]. San Diego: Elsevier; 2012 [cited 2024 Apr 28]. pp. 39–45. <https://www.sciencedirect.com/science/article/pii/B97801238468460001X>
- Luque A, Silveira CB. Quantification of Lysogeny caused by phage coinfections in Microbial communities from Biophysical principles. *mSystems.* 2020;5:e00353–20.
- Hatfull GF, Dedrick RM, Schooley RT. Phage therapy for antibiotic-resistant bacterial infections. *Annu Rev Med.* 2022;73:197–211.
- Górski M&KD. A. Engineered Bacteriophage Therapeutics: rationale, challenges and future. *BioDrugs Clin Immunotherapeutics Biopharmaceuticals Gene Therapy* [Internet]. 2021 [cited 2023 Jan 16];35. <https://pubmed.ncbi.nlm.nih.gov/33881767/>
- Strathdee SA, Hatfull GF, Mutalik VK, Schooley RT. Phage therapy: from biological mechanisms to future directions. *Cell.* 2023;186:17–31.
- Laanto E, Mäkelä K, Hoikkala V, Ravantti JJ, Sundberg L-R. Adapting a phage to combat phage resistance. *Antibiot (Basel).* 2020;9:291.
- Georjon H, Bernheim A. The highly diverse antiphage defence systems of bacteria. *Nat Rev Microbiol.* 2023;21:686–700.
- Labrie SJ, Samson JE, Moineau S. Bacteriophage resistance mechanisms. *Nat Rev Microbiol.* 2010;8:317–27.
- Nayak T, Kakkar A, Singh RK, Jaiswal LK, Singh AK, Temple L, et al. Isolation and characterization of a novel mycobacteriophage Kashi-VT1 infecting *Mycobacterium* species. *Front Cell Infect Microbiol.* 2023;13:1173894.
- Fei B, Li D, Liu X, You X, Guo M, Ren Y, et al. Characterization and genomic analysis of a broad-spectrum lytic phage HZ2201 and its antibiofilm efficacy against *Pseudomonas aeruginosa*. *Virus Res.* 2023;335:199184.
- Glonti T, Pirnay J-P. In Vitro techniques and measurements of phage characteristics that are important for phage therapy success. *Viruses.* 2022;14:1490.
- Khan Mirzaei M, Nilsson AS. Isolation of phages for phage therapy: a comparison of Spot tests and efficiency of plating analyses for determination of host range and efficacy. *PLoS ONE.* 2015;10:e0118557.
- Coyne AJK, Stamper K, Kebriaei R, Holger DJ, El Ghali A, Morrisette T, et al. Phage cocktails with Daptomycin and Ampicillin eradicates Biofilm-embedded multidrug-resistant *Enterococcus faecium* with preserved phage susceptibility. *Antibiot (Basel).* 2022;11:1175.
- Kunz Coyne AJ, Stamper K, Bleick C, Kebriaei R, Lehman SM, Rybak MJ. Synergistic bactericidal effects of phage-enhanced antibiotic therapy against MRSA biofilms. *Microbiol Spectr.* 2024;12:e03212–23.
- Soontarach R, Sriramanote P, Voravuthikunchai SP, Chusri S. Antibacterial and Anti-biofilm Efficacy of Endolysin LysAB1245 against a panel of important pathogens. *Pharmaceuticals (Basel).* 2024;17:155.
- Yang C-H, Su P-W, Moi S-H, Chuang L-Y. Biofilm formation in *Acinetobacter baumannii*: genotype-phenotype correlation. *Molecules.* 2019;24:1849.
- Shenkutie AM, Yao MZ, Siu GK, Wong BKC, Leung PH. Biofilm-induced antibiotic resistance in clinical *Acinetobacter baumannii* isolates. *Antibiot (Basel).* 2020;9:817.
- Khalil MAF, Ahmed FA, Elkhateeb AF, Mahmoud EE, Ahmed MI, Ahmed RI, et al. Virulence characteristics of biofilm-forming *Acinetobacter baumannii* in clinical isolates using a *Galleria mellonella* model. *Microorganisms.* 2021;9:2365.
- Granata G, Taglietti F, Petrosillo N. Tackling *Acinetobacter baumannii*. *J Clin Med.* 2023;12:5168.
- Giammanco A, Calà C, Fasciana T, Dowzicky MJ. Global Assessment of the activity of Tigecycline against Multidrug-Resistant Gram-negative pathogens between 2004 and 2014 as part of the Tigecycline evaluation and Surveillance Trial. *mSphere.* 2017;2:e00310–16.
- Ibrahim S, Al-Saryi N, Al-Kadmy IMS, Aziz SN. Multidrug-resistant *Acinetobacter baumannii* as an emerging concern in hospitals. *Mol Biol Rep.* 2021;48:6987–98.
- Rt S, Jj BB, A H-M G et al. J L, L L. Development and use of personalized bacteriophage-based therapeutic cocktails to treat a patient with a disseminated resistant *Acinetobacter baumannii* infection. *Antimicrobial Agents Chemotherapy* [Internet]. 2017 [cited 2023 Jan 16];61. <https://pubmed.ncbi.nlm.nih.gov/28807909/>
- Wu N, Dai J, Guo M, Li J, Zhou X, Li F, et al. Pre-optimized phage therapy on secondary *Acinetobacter baumannii* infection in four critical COVID-19 patients. *Emerg Microbes Infect.* 2021;10:612–8.
- Rao S, Betancourt-Garcia M, Kare-Opaneye YO, Swierczewski BE, Bennett JW, Horne B et al. Critically ill patient with multidrug-resistant *Acinetobacter baumannii* respiratory infection successfully treated with intravenous and nebulized bacteriophage therapy. *Antimicrob Agents Chemother.* 2022;66:e00824–21.
- Nir-Paz R, Gelman D, Khouri A, Sisson BM, Fackler J, Alkalay-Oren S, et al. Successful treatment of Antibiotic-resistant, poly-microbial bone infection with bacteriophages and antibiotics Combination. *Clin Infect Dis.* 2019;69:2015–8.
- Vandamme EJ. Phage therapy and phage control: to be revisited urgently!! *J Chem Technol Biotechnol.* 2014;89:329–33.

39. Jeon J, D'Souza R, Pinto N, Ryu C-M, Park J, Yong D, et al. Characterization and complete genome sequence analysis of two myoviral bacteriophages infecting clinical carbapenem-resistant *Acinetobacter baumannii* isolates. *J Appl Microbiol.* 2016;121:68–77.
40. Hussain A, Kousar S, Ullah I, Zulfiqar A, Ali HA, Manzoor A, et al. Investigations on Acinetophage, QAB 3.4, Targeting extensively drug-resistant *Acinetobacter baumannii* isolates. *Infect Drug Resist.* 2021;14:4261–9.
41. Cobián Güemes AG, Le T, Rojas MI, Jacobson NE, Vilella H, McNair K, et al. Compounding *Achromobacter* phages for therapeutic applications. *Viruses.* 2023;15:1665.
42. Kaushik V, Tiwari M, Joshi R, Tiwari V. Therapeutic strategies against potential antibiofilm targets of multidrug-resistant *Acinetobacter baumannii*. *J Cell Physiol.* 2022;237:2045–63.
43. Bhartiya SK, Prasad R, Sharma S, Shukla V, Nath G, Kumar R. Biological therapy on infected traumatic wounds: a case-control study. *Int J Low Extrem Wounds.* 2022;15347346211072779.
44. Gayoso CM, Mateos J, Méndez JA, Fernández-Puente P, Rumbo C, Tomás M, et al. Molecular mechanisms involved in the response to desiccation stress and persistence in *Acinetobacter baumannii*. *J Proteome Res.* 2014;13:460–76.
45. Tang Z, Li X, Wang X, Zhang C, Zou L, Ren H et al. Characterization and genomic analysis of a novel lytic phage DCp1 against *Clostridium perfringens* biofilms. *Int J Mol Sci [Internet].* 2023 [cited 2024 May 6];24. <https://www.ncbi.nlm.nih.gov/pmc/articles/PMC9965233/>
46. Ding Y, Huang C, Zhu W, Li Z, Zhang Y, Wang J, Pan H, Li H, Wang X. Characterization of a novel Jerseyvirus phage T102 and its inhibition effect on biofilms of multidrug-resistant *Salmonella*. *Virus research [Internet].* 2023 [cited 2024 May 6];326. <https://pubmed.ncbi.nlm.nih.gov/36717022/>
47. Jiang L, Xu Q, Wu Y, Zhou X, Chen Z, Sun Q et al. Characterization of a Straboviridae phage vB\_AbaM-SH1 and its inhibition effect on biofilms of *Acinetobacter baumannii*. *Front Cell Infect Microbiol [Internet].* 2024 [cited 2024 Apr 17];14. <https://www.ncbi.nlm.nih.gov/pmc/articles/PMC10958429/>
48. Liu B, Guo Q, Li Z, Guo X, Liu X. Bacteriophage endolysin: a powerful weapon to control bacterial biofilms. *Protein J.* 2023;42:463–76.
49. Huang Z, Zhang Z, Tong J, Malakar PK, Chen L, Liu H, et al. Phages and their lysins: toolkits in the battle against foodborne pathogens in the postantibiotic era. *Compr Rev Food Sci Food Saf.* 2021;20:3319–43.
50. Rahman MU, Wang W, Sun Q, Shah JA, Li C, Sun Y, et al. Endolysin, a Promising solution against Antimicrobial Resistance. *Antibiot (Basel).* 2021;10:1277.
51. Yuan Y, Li X, Wang L, Li G, Cong C, Li R, et al. The endolysin of the *Acinetobacter baumannii* phage vB\_AbaP\_D2 shows broad antibacterial activity. *Microb Biotechnol.* 2020;14:403–18.
52. Lendel AM, Antonova NP, Grigoriev IV, Usachev EV, Gushchin VA, Vasina DV. Biofilm-disrupting effects of phage endolysins LysAm24, LysAp22, LysECD7, and LysSi3: breakdown the matrix. *World J Microbiol Biotechnol.* 2024;40:186.
53. Ahammad T, Khan RH, Sahu ID, Drew DL, Faul E, Li T, et al. Pinholin S21 mutations induce structural topology and conformational changes. *Biochim Biophys Acta Biomembr.* 2021;1863:183771.
54. Xiang Y, Wang S, Huang H, Li X, Li H, Tu Y, Wei Y, Song F, Ji X, A novel holin from an *Enterococcus faecalis* phage and application in vitro and in vivo. *Microbial pathogenesis [Internet].* 2024 [cited 2024 May 6];186. <https://pubmed.ncbi.nlm.nih.gov/38048838/>
55. Bartal C, Rolston KVI, Neshler L. Carbapenem-resistant *Acinetobacter baumannii*: colonization, infection and current treatment options. *Infect Dis Ther.* 2022;11:683–94.
56. Mei H, Yang T, Wang J, Wang R, Cai Y. Efficacy and safety of tigecycline in treatment of pneumonia caused by MDR *Acinetobacter baumannii*: a systematic review and meta-analysis. *J Antimicrob Chemother.* 2019;74:3423–31.
57. Qureshi ZA, Hittle LE, O'Hara JA, Rivera JI, Syed A, Shields RK, et al. Colistin-resistant *Acinetobacter baumannii*: beyond carbapenem resistance. *Clin Infect Dis.* 2015;60:1295–303.
58. Jansen M, Wahida A, Latz S, Krüttgen A, Häfner H, Buhl EM, et al. Enhanced antibacterial effect of the novel T4-like bacteriophage KARL-1 in combination with antibiotics against multi-drug resistant *Acinetobacter baumannii*. *Sci Rep.* 2018;8:14140.
59. Tan X, Chen H, Zhang M, Zhao Y, Jiang Y, Liu X, et al. Clinical experience of personalized phage therapy against Carbapenem-Resistant *Acinetobacter baumannii* Lung infection in a patient with Chronic Obstructive Pulmonary Disease. *Front Cell Infect Microbiol.* 2021;11:631585.
60. Ambroa A, Blasco L, López M, Pacios O, Bleriot I, Fernández-García L, et al. Genomic Analysis of Molecular Bacterial Mechanisms of Resistance to phage infection. *Front Microbiol.* 2022;12:784949.
61. Klumpp J, Dunne M, Loessner MJ. A perfect fit: bacteriophage receptor-binding proteins for diagnostic and therapeutic applications. *Curr Opin Microbiol.* 2023;71:102240.
62. Egidio JE, Costa AR, Aparicio-Maldonado C, Haas P-J, Brouns SJJ. Mechanisms and clinical importance of bacteriophage resistance. *FEMS Microbiol Rev.* 2021;46:fuab048.
63. Timoshina OY, Kasimova AA, Shneider MM, Arbatsky NP, Shashkov AS, Shelonkov AA, et al. Loss of a Branch Sugar in the *Acinetobacter baumannii* K3-Type capsular polysaccharide due to frameshifts in the *gtr6* glycosyltransferase gene leads to susceptibility to phage APK37.1. *Microbiol Spectr.* 2023;11:e0363122.
64. Arbatsky NP, Kasimova AA, Shashkov AS, Shneider MM, Popova AV, Shagin DA, et al. Involvement of a phage-encoded *wzy* protein in the polymerization of K127 units to form the Capsular Polysaccharide of *Acinetobacter baumannii* isolate 36-1454. *Microbiol Spectr.* 2022;10:e0150321.
65. Gordillo Altamirano F, Forsyth JH, Patwa R, Kostoulias X, Trim M, Subedi D, et al. Bacteriophage-resistant *Acinetobacter baumannii* are resensitized to antimicrobials. *Nat Microbiol.* 2021;6:157–61.
66. Kenyon JJ, Hall RM. Variation in the complex carbohydrate biosynthesis loci of *Acinetobacter baumannii* genomes. *PLoS ONE.* 2013;8:e62160.
67. Wang X, Loh B, Gordillo Altamirano F, Yu Y, Hua X, Leptihn S. Colistin-phage combinations decrease antibiotic resistance in *Acinetobacter baumannii* via changes in envelope architecture. *Emerg Microbes Infect.* 2021;10:2205–19.
68. Morrisette T, Kebriaei R, Lev KL, Morales S, Rybak MJ. Bacteriophage therapeutics: a primer for clinicians on phage-antibiotic combinations. *Pharmaco-therapy.* 2020;40:153–68.
69. Chan BK, Siström M, Wertz JE, Kortright KE, Narayan D, Turner PE. Phage selection restores antibiotic sensitivity in MDR *Pseudomonas aeruginosa*. *Sci Rep.* 2016;6:26717.

## Publisher's note

Springer Nature remains neutral with regard to jurisdictional claims in published maps and institutional affiliations.